RESEARCH PAPER

Investigating oxygen transport efficiencies in precision-cut liver slice-based organ-on-a-chip devices

Martin G. Christensen[1] · Chris Cawthorne[2] · Charlotte E. Dyer[2] · John Greenman[2] · Nicole Pamme[1]

Abstract

Microfluidic 'organ-on-a-chip' devices hold great potential for better mimicking the continuous flow microenvironment experienced by tissue and cells in vivo, thereby ensuring realistic transport of nutrients and elimination of waste products. However, the mass transport of oxygen, which arguably is the most critical nutrient due to its inherently low solubility in water, is rarely assessed. To this aim, the suitability of various precision-cut liver slice (PCLS) microfluidic devices for the defined maintenance of oxygen mass transport were evaluated using COMSOL simulations, leading to the development of a novel, optimised design to provide defined in vivo oxygenation conditions within an organ-on-a-chip system. Simulations found that the proposed device was capable of maintaining 43% of the tissue slice volume within the physiological range of the liver against 18% for the best performing literature device. The optimal device architecture derived from the modelling was then fabricated and its operation confirmed with an LDH assay. These simulation results form the basis for a greater understanding of not just the challenges involved in designing organ-on-a-chip devices, but also highlight issues that would arise from the incorporation of additional organs, as research progresses towards complete human-on-a-chip model systems.

Keywords Organ-on-chip · Liver metabolism · Oxygen tension · COMSOL modelling

1 Introduction

Pharmaceutical companies face great challenges in their endeavour to translate biological knowledge into novel drugs. It has been estimated that it takes upwards of 12 years to get a drug into market with an associated cost of about $12 billion dollars (Visk 2015). However, the road that pharmaceutical companies have to travel to develop and release a drug successfully into the market is filled with challenges. Novel drug candidates face exceedingly high attrition rates of 90% when attempting to transition from clinical trials into the market (Visk 2015).

The liver is the primary organ attributed to many of these drug development failures since its metabolic specialisation renders it susceptible to drug-induced liver injury (DILI) (Patel et al. 2012; Kullak-Ublick et al. 2017; Iorga et al. 2017). This occurs even though preclinical liver model systems (microsomes, hepatocytes, liver slices and animals) for a long time have constituted an integral part in the drug development pipeline. The failure of current platforms to allow eventual drug failures to slip through the net and proceed into clinical trials can be partly attributed to their lack of predictability arising from a lack of relevant components and pathways in the particular models as well as shortcomings of the interrogation platform (Esch et al. 2014). In addition, there is a move to reduce animal use therefore, the demand from the pharmaceutical industry for better preclinical in vitro system which more accurately predict the in vivo properties of drug candidates is extremely strong (Usta et al. 2015).

Organ-on-a-chip devices couple well-established biological model systems with the flow control and microenvironment manipulation offered by microfluidics to create better in vivo mimicking conditions. Much attention has been directed at utilising cell-lines (Cheng et al. 2006; Rodrigues et al. 2008; Ges and Baudenbacher 2010a,b; Hiatt et al. 2012; Weltin et al. 2014) or artificial cell aggregates, i.e., spheroids (Misun et al.2015, 2016; Ortega-Prieto et al. 2018). However, these do not fully reflect the inherent

✉ Nicole Pamme
  n.pamme@hull.ac.uk

[1] Department of Chemistry and Biochemistry, University of Hull, Cottingham Road, Hull HU6 7RX, UK

[2] Department of Biomedical and Forensics Sciences, University of Hull, Cottingham Road, Hull HU6 7RX, UK

complexity of native organs which feature a multitude of distinct cell types, extracellular matrix and spatial organisation. The liver is comprised of at least 7 distinct cell types (Gupta 2018) and more than 15 different extracellular matrix components (Bedossa and Paradis 2003). Thus, some groups have investigated organ biopsies in the form of precision-cut tissue slices (PCTS) for organ-on-a-chip devices, as these are directly obtained from the target organ (Blake et al. 2007; Rambani et al. 2009; Midwoud et al. 2011; Chang et al. 2012; Astolfi et al. 2016) and, therefore, more accurately maintain the composition and organisation of the cell types and extracellular matrix. As compared to cell-monolayers, the tissue slices contain multiple layers and typically range in 100–250 µm thickness (Graaf et al. 2007). These relatively large dimensions imply that the penetration and depletion of oxygen in the tissue slice should be given consideration.

Oxygenation is well established as an important culture parameter for maintaining both the function and viability of biological systems (Camp and Capitano 2007). Although the oxygen content in the air is approximately 21%, the normoxic conditions in vivo are tissue specific, ranging from as low as 0% in the bone marrow to 14% in well-perfused tissues such as the liver, heart and lungs (Ivanovic 2009; Adams 2012). In vivo the task of oxygenating tissues is undertaken by the oxygen binding hemoglobins, which circumvent the inherently low solubility of molecular oxygen in water, which at 37 °C under standard atmospheric conditions is approximately 0.2 mM. The hemoglobin acts as an oxygen reservoir that replenishes the pool of soluble oxygen available for cellular consumption. In vitro, however, researchers mostly rely on high carbogen atmospheres, e.g. 95% O_2 and 5% CO_2 to provide PCLS with an adequate supply of oxygen during culture. The importance of mimicking in vivo liver oxygen tensions (0.042–0.091 mM) has been highlighted via improved maintenance of cellular functions such as those involved in drug metabolising pathways (Jungermann and Keitzmann 1996; Jungermann and Kietzmann 2000; Camp and Capitano 2007; Guo et al. 2017). However, little attention has been given to assessing the mass transport of oxygen in tissue slice microfluidic devices, wherein, the low media perfusion contact length to tissue volume ratio constitute a challenge both in terms of ensuring adequate oxygen and maintaining regions within a narrow window matching those found in vivo. Here, simulations were performed to assess tissue oxygenation within several published liver-on-chip devices and, based on these findings, an optimised device for maintenance of PCTS for liver-on-chip was developed. The modelling was tested by preliminary experimental studies.

2 Experimental

2.1 Modelling

Computer simulations were carried out in COMSOL Multiphysics 5.2 (COMSOL AB). Mesh convergence assessments were performed on simulation geometries to determine appropriate mesh settings in each of the simulations. COMSOL's physics for laminar flow and transport of diluted chemical species were employed for the simulations. The computed flows were calculated based on the assumption of a non-compressible fluid and with a no-slip boundary condition imposed on both the surfaces of the tissue slice and the wall domains.

The transport of nutrients in the simulation was described by the generic diffusion equation as given in Eq. 1, R is a reaction term, $\vec{u}$ is the velocity field and c is the concentration of the species.

$$\frac{\partial c}{\partial t} = \nabla \cdot (D\nabla c) - \nabla \cdot (\vec{u}c) + R \tag{1}$$

To account for the consumption of various species, reaction kinetics were implemented. The consumption of oxygen was calculated with Michaelis–Menten reaction kinetics (Eq. 2), V_{max} is the maximum consumption rate, c the concentration and K_m is the Michaelis–Menten constant.

$$R = \frac{V_{Max}C}{K_M + C}\delta(C > C_{Crit}) \tag{2}$$

Furthermore, to account for cellular processes such as necrosis, which would occur when the local oxygen concentrations drop below a certain threshold under which cells would no longer be considered viable, a δ factor was implemented based on COMSOL's smoothed Heaviside function [flc1hs (step, scale)] (Buchwald 2011). The function eliminates the reaction term for the cellular consumption by going to zero when $C < C_{crit}$ is valid and being equal to one for C_{crit}, thus ensuring that cells which occupy a region of space below the C_{crit} will not consume oxygen. The necrotic oxygen tension threshold C_{crit} for the liver tissue was 2.64 10^{-3} mol m^{-3} based on Mattei et al. (Chang et al. 2014). A maximum consumption rate of 0.059 mol s^{-1} m^{-3} and a Michaelis–Menten constant of 0.0033 mol m^{-3} were utilised in the simulations based on consumption measurements performed by Buerk et al. with implantable micro-oxygen electrodes in liver and brain slices (Buerk and Saidel 1978).

Due to the inherently low flow permeability of tissue, this transport mechanic was neglected apart from in those devices wherein geometrical constraints force the flow directly through the tissue. These utilised a porosity of 0.4 and a permeability of 1·10^{-11} m^2 as derived from brain tissue (Mattei et al. 2014). As no established porosity and

permeability parameters could be gathered for instance where matrigel was used to encapsulate tissues, it was assigned the same values as the tissue slices.

The mesh settings and the mesh convergence assessment used to establish these for the simulations are described in ESI1.

2.2 Device design and fabrication

The microfluidic chip device, designed based on the findings from the COMSOL modelling, consisted of a top layer made from polystyrene (PS), a tissue layer made from PS and a bottom layer from Poly(methyl methacrylate) (PMMA) (Fig. 1 and ESI2). Two PDMS gas exchange membranes were held in close proximity to the tissue slice, which was harboured within a tissue unit (Fig. 2).

The top layer was 4 mm thick and featured CNC milled holes (Datron M7, Datron, Germany) for bolts (4.35 mm diameter), holes for inlet and outlet tubing (2.35 mm), holes for purge valves (2 mm) and a "breathing window" for the

PDMS gas exchange (4 mm) (figure S2.1). A PDMS assembly consisting of a 3 mm thick PDMS slab which had been through-holed with a 4 mm punch and attached to a 50 μm thick layer was aligned and attached to the top layer so that the 3 mm PDMS through-hole matched the breathing window opening in the top layer. The middle tissue layer was 0.8 mm thick with a 28 mm long and 4.2 mm wide through-cut fluidic channel with a central 13.5 mm wide circular and 0.525 mm deep recess for the positioning of the tissue unit carrier harbouring the PCLS (fig S2.2). To enclose the bottom part of the through-cut fluidic channel a 50 μm thick PDMS layer was attached to the tissue layer. The bottom layer was 9.5 mm thick with 4.35 mm wide bolt holes and with a 0.6 mm deep oval recess for accurate positioning of the tissue layer (figure S2.3). The top PS and bottom PMMA layer parts had 4 mm wide centrally located holes serving as PDMS breathing windows for the PCLS.

The tissue unit featured two 50 μm thick nylon meshes with 60 μm pore size laser-cut to size from a Falcon cell strainer membrane (Thermo Fisher Scientific) as well as two

Fig. 1 Schematic of the PDMS sandwich device featuring the three main components of the chip. (Tissue unit is not shown)
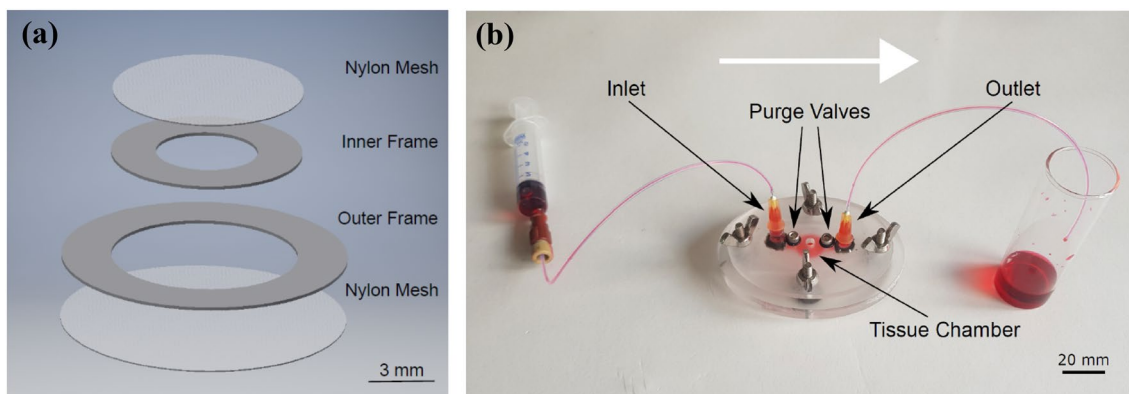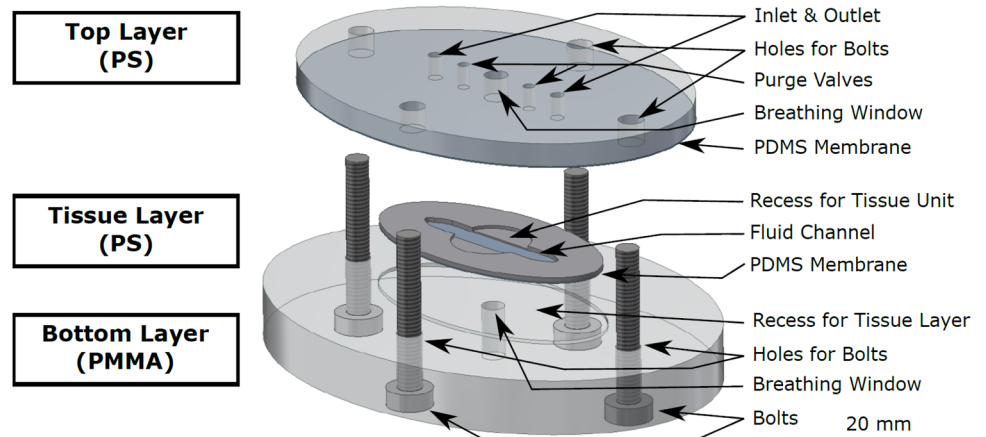

Fig. 2 CAD illustration of the tissue unit assemblies and manufactured device. **a** Exploded view of a tissue unit consisting of two 50-μm thick nylon meshes and two separate PMMA layers. A nylon mesh membrane was bonded directly onto each PMMA layer by chlo-roform vapour exposure, to create the two individual parts of the tissue unit. **b** Photo of the complete chip with red dye solution pumped through to test for leakages

separate PMMA layers (Fig. 2, ESI3). These PMMA layers were cut into inner and outer frames and the nylon mesh was bonded directly onto these by chloroform vapour exposure. The tissue layer incorporated a side step for positioning of the PCLS, thus simultaneously ensuring that the tissue slice was maintained at a mid-height position and directly beneath the openings of the PDMS breathing windows. The device was fully assembled as laid out in ESI4.

To maintain the applied atmosphere, a 2 L glass vessel was fitted with two gas line adapters and ports for suba rubber septa (Chemglass Life Sciences) (Fig. 3). Incoming gas was directed through a gas washer to humidify the inflow into the vessel, whereafter the gas would exit via the second gas line adapter into a purging vessel. The humidification of the gas inflow was done to prevent the potentially adverse evaporation of liquid through the PDMS membranes of the chip and the silicone rubber gas exchange tubing (ID 0.6 mm, wall thickness 0.35 mm) (Hilltop Products Ltd). The glass vessel was housed within a commercial egg incubator (COVATUTTO) operating at a temperature of 37 °C.

2.3 PCLS experiments on-chip

2.3.1 Chemicals and buffers

PDMS was obtained from Dow Chemical Company. Williams medium E (WME) was bought from Life Technologies Ltd, fetal bovine serum and KCl were bought from Thermo Fisher Scientific. D-Glucose, NaOH and NaCl were purchased from VWR. Agarose, $CaCl_2$, KH_2PO_4 $MgSO_4$ and HEPES were sourced from Sigma Aldrich.

Krebs–Henseleit buffer (KHB) for tissue slicing was prepared according to Graaf et al. (Graaf et al. 2010). The $1 \times KHB$ buffer solution had final concentrations of 2.5 mM $CaCl_2$, 118 mM NaCl, 1.1 mM $MgSO_4$, 1.2 mM KH_2PO_4, 25 mM $NaHCO_3$, 25 mM D-Glucose, 10 mM HEPES. The solution was placed on ice and oxygenated with a gas mixture consisting of 95% O_2 and 5% CO_2 and adjusted to a pH of 7.4 with NaOH.

2.3.2 Process to cut and insert liver slice

The animal work was performed under ethics application U2017 002 as approved by the ethical committee at the University of Hull. The mice were all females and derived from the C57BL/6 J and Rhobtb3 ± strains. The sacrifice was performed by CO_2 inhalation, whereafter the liver was excised and immediately submerged into ice-cold oxygenated (95% O_2 and 5% CO_2) KHB. Preparation and slicing of liver tissue was done according to the protocol of Graaf et al. (2010).

Fresh liver tissue as obtained after sacrifice was placed on a cutting mat consisting of a Petri-dish filled with 3% agarose. The tissue was covered with ice-cold KHB. A lobe of the liver was cut away and blotted on a piece of tissue to remove water whereafter it was glued onto the specimen stage with a Loctite Liquid Superglue 3G cyanoacrylate adhesive (Henkel Ltd). The glue was given a minute to set whereafter it was mounted on the Vibratome 1200S (Leica) stage in a buffer tray filled with ice-cold oxygenated KHB. The vibratome settings for the slicing were a slice thickness of 150 μm and a blade clearance angle of 18° and feed speed of 0.08 mm s^{-1}. Based on mass transport considerations this particular thickness was selected as it is in the low end of the reported PCLS thickness values in the literature (Graaf et al. 2007).

The precision cut tissue sheets (see ESI5) were transferred from the tray with a spatula. Slices were either used to generate uniformly sized cylindrical PCLS with a 4 mm

Fig. 3 Schematic of the experimental setup used in the PCLS incubation experiments with the proposed device
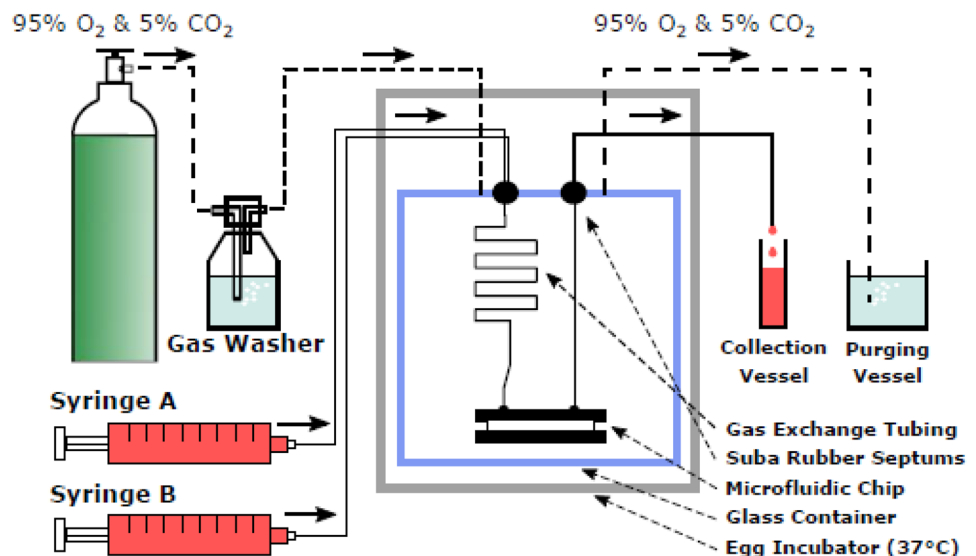
biopsy punch (Miltex) or used directly without any additional processing. The punching was performed by placing the tissue sheets flat on a 3% agarose Petri-dish filled with ice-cold oxygenated KHB. The PCLS were subsequently transferred with a cut plastic Pasteur pipette into a 50-mL tube filled with 5-mL ice-cold oxygenated KHB until use. After use tools were cleaned with EtOH and autoclaved (126 °C, 11 min).

2.3.3 Experimental process

Microfluidic chips were either autoclaved or thoroughly flushed with EtOH before each experiment, and chip and workspace surfaces were wiped down with EtOH to minimise the possibility of bacterial contamination. The cell medium consisted of WME supplemented with FBS and HEPES to final concentrations of 10% and 10 mM, respectively. For antibiotics, penicillin, streptomycin, and neomycin were added at final concentrations of 50 and 100 μg L^{-1}, respectively. WME was selected since it a frequently used medium for PCLS (Graaf et al. 2010).

The medium was loaded into 20-mL or 50-mL syringes in a class two biological safety cabinet. The syringes were mounted on a syringe pump and connected to the microfluidic chips, which were housed inside an egg incubator unit set to maintain a temperature of 37 °C (ESI6). The length of the tubing was chosen so that the surface areas were sufficiently large to heat up the medium from room temperature to 37 °C before it reached the tissue. One PCLS was then loaded into the tissue cavity of each microfluidic chip and the perfusion was initiated. The first collection of the effluent from the individual chips was done at the 2 h time point, whereafter all subsequent ones were collected at 24-h intervals.

Conventional tissue slice incubation on PICMORG50 well plate inserts (EMD Millipore Corporation) in six-well plates were run in parallel with the microfluidic experiments for comparison. Three slices were used for each well insert with 1.1 mL WME and medium changes were performed on the same schedule as for the microfluidic chips.

2.3.4 Measurements

Lactate dehydrogenase (LDH) was used as a biomarker for cell death by monitoring the release of this enzyme into the effluent. LDH content in tissue lysates was additionally assessed to determine the viability of the PCLS at the end of the incubations. Individual PCLS were collected and initially fragmented into smaller bits by vigorous pippetting in 500 μL 1%(v/v) Triton X-100 and were then left on ice for 45 min. Solutions were then cleared by centrifugation at 12,000g for 10 min, after which the supernatants were collected and diluted 1:16 with water to get within the linear range of the LDH assay. The LDH was measured with a Pierce^{TM} LDH cytotoxicity assay kit at wavelength of 490 nm according to the manufacturer's guidelines.

3 Results and discussion

3.1 COMSOL modelling of published devices

COMSOL simulations were conducted to investigate how the transport efficiency of oxygen would theoretically compare across different published platforms, as well as with the herein proposed chip design. Several PCLS-based microfluidic devices have been published (Midwoud et al. 2010,2011; Sivashankar et al. 2012; Wu et al. 2012). These devices can broadly be separated into three different design categories (Fig. 4): (a) a PDMS flow-through perfusion approach, in which fluid is pushed through a tissue slice (Midwoud et al. 2010, 2011), (b) an intra-perfusion approach, in which piercing needles deliver a flow of medium directly into the core of the tissue slice and (Sivashankar et al. 2012), (c) an approach employing perfusion from a narrow channel above or below the tissue (Wu et al. 2012).
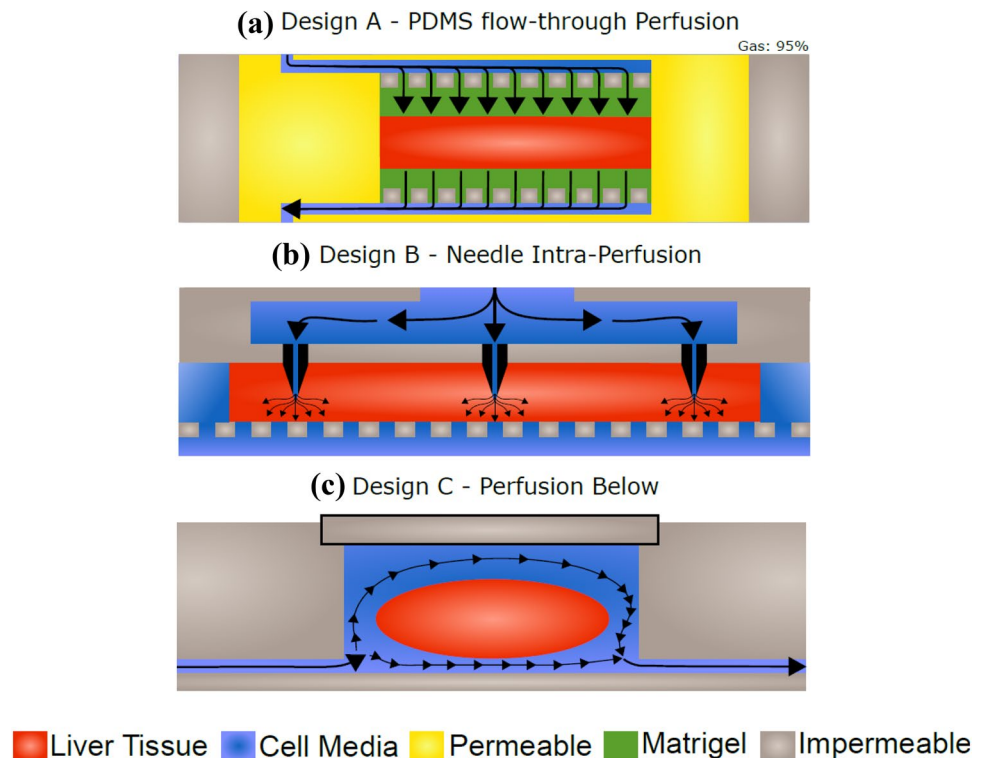
3.2 PDMS flow-through approach (Midwoud et al. 2010, 2011)

The device designed by Midwoud et al. featured a 4 mm wide and 250 μm thick PCLS encased in a Matrigel slab held together by two 10-μm thick porous polycarbonate membranes. The flow at a rate of 10 μL min^{-1} entered the chip through a single inlet at the top, passed through the tissue slice and then exited via a single outlet. For gas exchange purposes, 250-μm thick PDMS membranes were attached at the top and bottom of the device with the entire chip being placed in an incubator containing a 95% oxygen atmosphere.

The COMSOL simulation of oxygen concentrations within the device reveal that the fluid is fully saturated (1017 mM) in the upper half of the device near the inlet and top gas exchange membrane region as shown in (Fig. 5a, b). However, as the flow progresses downward towards the tissue slice, a significant oxygen concentration gradient is established in the vertical direction. Near the bottom of the chip, which harboured the second PDMS gas exchange membrane, the partially depleted oxygen in the flow stream can be observed to rapidly equilibrate again with the external oxygen atmosphere as it progresses towards the outlet.

The results highlight the geometrical dependence of gas exchange membranes. For oxygen mass transport through a PDMS membrane to occur, the liquid immediately adjacent to the PDMS/liquid interface must have an oxygen saturation < 100%. Furthermore, in this particular chip design approach, it is crucial to position the tissue slice of a certain

Fig. 4 Schematic drawings of microfluidic incubation chips utilised for liver tissue experiments. **a** Cylindrical PDMS flow-through perfusion PDMS chip wherein the PCLS is encased in matrigel. **b** Needle intra-perfusion chip. **c** Glass chip based on perfusing the tissue from above and beneath

(a) Design A - PDMS flow-through Perfusion
Gas: 95%

(b) Design B - Needle Intra-Perfusion

(c) Design C - Perfusion Below

■ Liver Tissue ■ Cell Media ■ Permeable ■ Matrigel ■ Impermeable

diameter precisely in the flow cylinder of the same diameter; any potential geometrical mismatch would lead to fluid being directed around rather than through the porous tissue slice.

One potential issue with this design approach, wherein the flow is guided through the slice, is that it is likely to cause changes to the tissue morphology via the formation of distinct flow paths going through the tissue slices. This has been observed in chips utilising the same approach. Rambani et al. found that flow paths and associated cell death in their vicinities occurred in brain slices when flow rates of greater than 20 μL h^{-1} were utilised (Rambani et al. 2009). This flow rate corresponded to a flow velocity of 7.86×10^{-4} mm s^{-1}, significantly lower than the 1.3×10^{-2} mm s^{-1} utilised by Midwoud et al. In comparison, the interstitial flow in vivo, which runs between the capillary/lymphatic systems and drain tissues, has a flow velocity within the range of $0.1–2 \times 10^{-4}$ mm s^{-1} (Khong et al. 2007). In addition, as these flow paths represent areas exhibiting a significantly lower flow resistance compared to the bulk porous volume of the surrounding tissue mass, a disproportionately higher magnitude of the flow will go through these formed flow paths, than would have done so otherwise. This would render void one of the underlying assumptions of the simulations, namely that the properties of the tissue volume can be modeled as being a uniform isotropic mass. However, it would be possible to accommodate such paths in a model granted that these generated flow paths are uniformly scattered throughout the tissue volume and provided that the change in permeability was known.

Piercing needles (Sivashankar et al. 2012) were utilised in the second design approach to deliver nutrients directly into the core of the tissue to overcome mass transport limitations in thick tissue slices. The device employed seven needles with an outer and inner diameter of 300 μm and 150 μm, respectively, arranged in a pattern with a central needle and the remaining equally spaced radially at a 2.5 mm distance. The needles delivered a combined flow rate of 1 mL min^{-1} of air saturated medium (225 μM) into a tissue slice of a diameter of 8 mm and a thickness of 1 mm dimensions. The effects of this approach can be been seen from the simulation (Fig. 5c, d). Highly oxygenated regions were found within a radius of approximately 1 mm from each of the needle injection points, as viewable when plotting the concentration along the radius of the tissue at mid-height (Fig. 5d). Within this region, the initial 500 μm experienced a mass transport influx of oxygen which was so significant that it was capable of overcoming the drain from the cellular consumption rate by maintaining the tissue volume at near fully saturated levels. However, mass transport limitations readily become evident further away from the needle sources where the oxygen tension levels can be observed to drop down below the critical threshold value.

The perfusion channel (Wu et al. 2012) geometry was based around maintaining a 4 mm^3 liver section with delivery nutrients at 2 μL min^{-1} via a narrow channel (190 μm
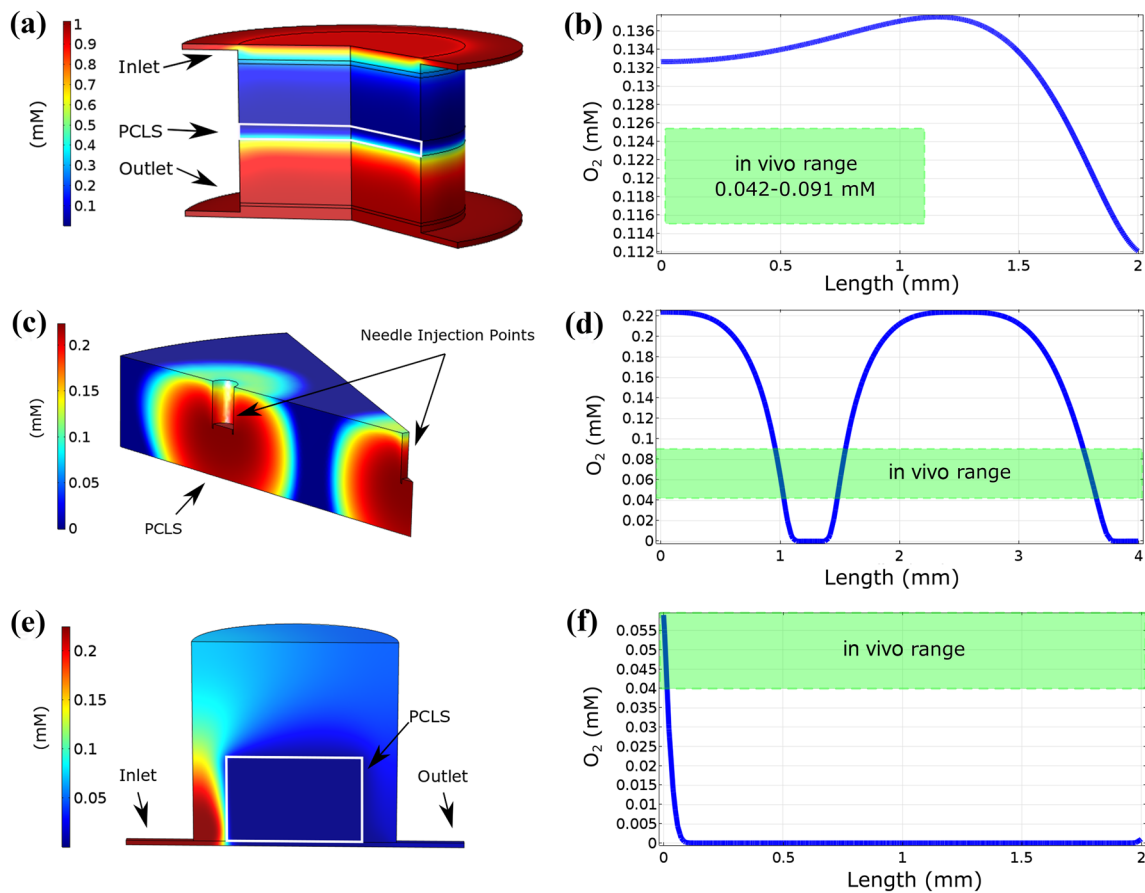
Fig. 5 **a** Oxygen concentration volume plot of the cylindrical PDMS flow-through Perfusion Device utilising a 95% oxygen saturated flow rate of 10 µL min^{-1} to maintain a 250 µm thick and 4 mm wide cylindrical PCLS (indicated with white lines). **b** Oxygen tensions within the tissue at mid-height for cylindrical flow-through device. **c** Oxygen concentration volume plot for needle intra-perfusion device utilising a flow rate of 1 mL min^{-1} to maintain a 1 mm thick and 8 mm wide cylindrical PCLS (30° section shown). **d** Oxygen tensions within the tissue at mid-height for needle device. **e** Oxygen concentration volume plot of the glass chamber perfusion device utilising a flow rate of 2 µL min^{-1} to maintain a 4 mm^3 PCLS (Indicated with white lines). **f** Oxygen tensions within the tissue at mid-height for chamber perfusion device. The green shaded regions on the line plots indicates the location of the in vivo oxygen tension range as found in the liver (colour figure online)

wide and 70 µm deep) running beneath the tissue chamber. From the oxygen consumption simulations (Fig. 5e, f) it can be observed that when the saturated flow enters the tissue chamber and comes into contact with the tissue section, the oxygen becomes gradually consumed as it progresses further towards the outlet. This gives rise to the formation of spatio-specific mass transport regions near the tissue interface, with the steepest oxygen concentration gradients and highest fluxes occurring at the front of the tissue near the chamber inlet. Less steep oxygen gradients are formed at the top and in particular rear areas of the tissue piece, due to lower flow velocities and progressively depleting oxygen concentrations. A plot of the oxygen tension levels, within the tissue at the mid-height line (Fig. 5f) reveals that adequate oxygen concentrations are only attained until a depth of approximately 100 µm,

thus leaving the vast majority of the tissue volume within an oxygen depleted zone.

3.3 COMSOL modelling of proposed PDMS sandwich device

To overcome oxygen transport limitations and better maintain the PCLS within the in vivo concentration range careful consideration must be given to materials and geometry. Based on the findings from the aforementioned COMSOL simulations, a novel microfluidic device was devised to achieve this.

Based on the fact that oxygen is the most limiting component of cell medium, due to its inherently low solubility, a geometry was envisioned wherein the flow would be continuously re-oxygenated along the flow direction. This would enable the sustaining of the tissue at a comparably
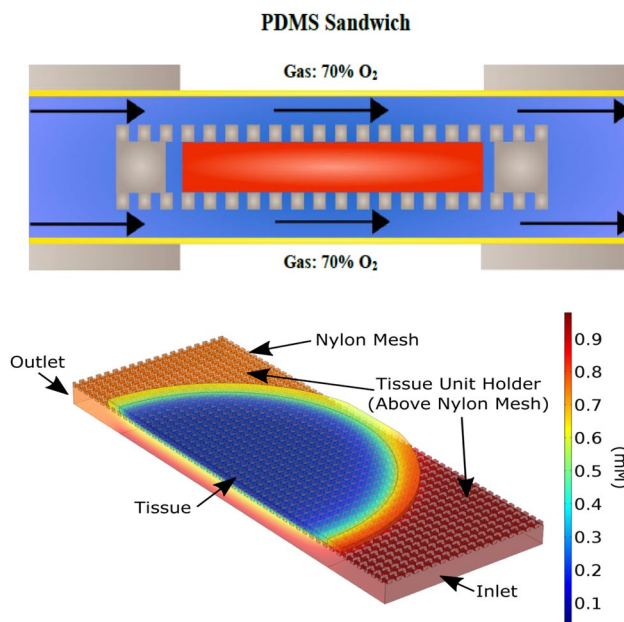
Fig. 6 **a** PDMS sandwich chip with the PCLS suspended between two PDMS membranes in a nylon mesh carrier. **b** Oxygen concentration plot of the device utilising an external gas atmosphere of 92% O2 and a flow rate of 4 μL min⁻¹. The 150-μm thick PCLS is suspended in a nylon mesh carrier between two PDMS gas exchange membranes. A quarter of the device is shown (Symmetry in the longitudinal and tangential direction)
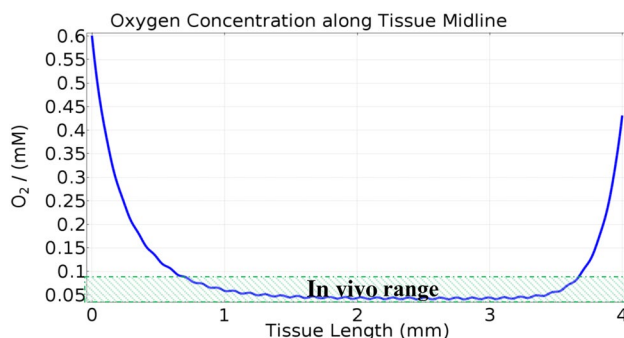

Fig. 7 Simulation of the oxygen tensions of a tissue slice incubated in the PDMS sandwich device as plotted along the length of the slice at the midheight. The device was operated with an external gas atmosphere of 92% O₂ and a flow rate of 4 μL min⁻¹

lower medium flow rate as compared to a compatible non-replenishing gas impermeable device. This allows for a tighter control of the tissue oxygen tension levels and would circumvent the imposition of steep tissue oxygen tension gradients along the flow direction. To achieve the aforementioned properties, the device was centred around two PDMS gas exchange membranes with the PCLS suspended mid-flow within a nylon mesh carrier. Fine control of the oxygen tension could be achievable by altering the composition of the surrounding atmosphere and the flow rate. The

oxygen concentration volume plot of the device revealed near homogeneous oxygen tension levels across the tissue with the exception being at the slice edges, where a steep increase was observed (Figs. 6 and 7). This oxygen tension gradient is based on the fact that the tissue slice edges would inevitably experience significantly higher oxygen tensions, due to the discontinuity in the balance between mass transport and cellular consumption. This design approach was experimentally realised as shown in Figs. 1, 2 and ESI2-4.

3.4 Comparison of simulation results of the PCLS-based microfluidic devices

The different chip designs were assessed in terms of their ability to maintain PCLS in physiologically relevant oxygen concentration ranges. Oxygen tension ranges were classified into four different groups: (i) low regions having concentrations below 0.042 mM, (ii) regions within the 0.042–0.091 mM range experienced in vivo (Jungermann and Kietzmann 2000), (iii) an intermediate high range of 0.091–0.15 mM and (iv) regions having oxygen tensions higher than 0.15 mM. Volume integration was performed over the tissues in terms of the effective concentrations and the resulting comparison of the devices (Fig. 8).

Mass transport issues were observed in all of the devices modelled, most significantly for the perfusion design wherein as much as 98.8% of the tissue volume fell within the low oxygen concentration range thus indicating a severe oxygen mass transport deficiency. Simulations of the flow-through approach and piercing needles approach showed a larger volume percentages in the physiologically relevant concentrations range, *i.e.,* 11% and 55%, respectively. The PDMS perfusion device displayed the largest tissue volume percentage within the in vivo range, among the devices from the literature, managing to achieve upwards of 11.4%.

Our proposed PDMS sandwich design performed significantly better as the tight control of the oxygen mass transport within the device was capable of maintaining approximately 43% of tissue within this range. However, this design had the highest tissue volume percentage with a value of 23% falling within the intermediate oxygen range, and the second highest occupying the high range at 33%. The cause of this was attributed to the mass transport discontinuity formed at the tissue/liquid interfaces at the edges of the tissue (Figs. 6 and 7). In comparison, relatively high proportions of the tissue volumes in the PDMS perfusion and piercing needle designs were also found to occupy regions within the high oxygen concentration range corresponding to 65% and 24%, respectively.

Fig. 8 Evaluation of chips based on calculated percentage of tissue occupying regions within the physiological range found in liver (0.042–0.091 mM), as well as those within low (< 0.042 mM), intermediate (0.091–0.15 mM) and high range oxygen concentrations (> 0.15 mM)
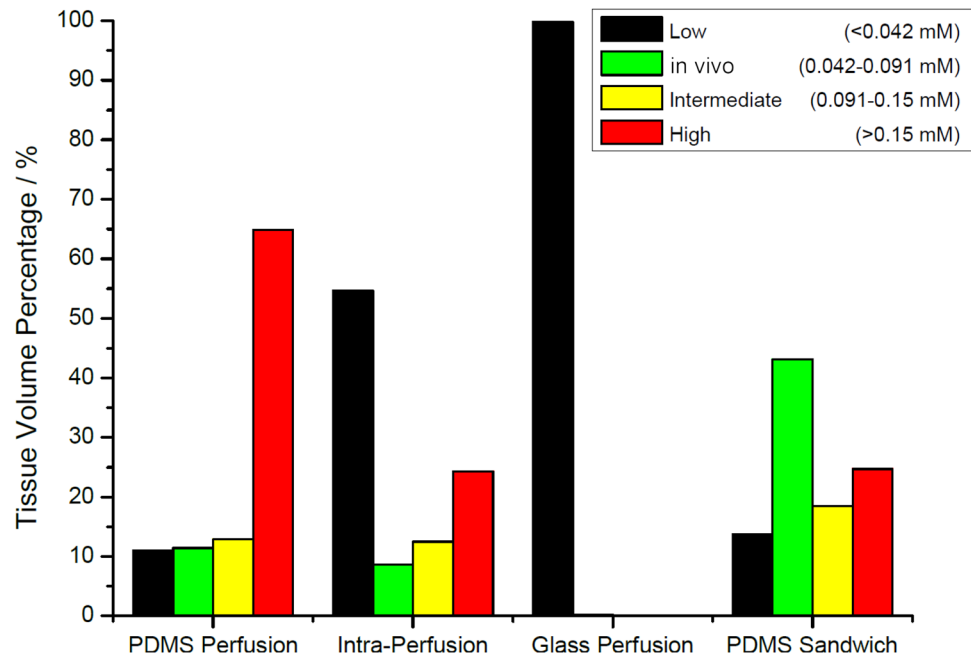
3.5 Operating parameters for proposed device

The device geometry derived from the COMSOL modelling (Figs. 6 and 7) was further investigated. As both the flow velocity and the applied gas atmospheres will impact the effective oxygen tensions experienced within an incubated PCLS, a sweep was conducted over these parameters to identify a suitable operating range for the device. The parameter combinations were evaluated based on the volume percentage of the PCLS which would be maintained within the physiological range (0.042–0.091 mM). As can be seen from the contour plot (Fig. 9), the optimum region which corresponded to a tissue volume of approximately 42% was found for flow rates of 0.5 µL min^{-1} combined with an atmosphere consisting of 80–90% oxygen. The usage of slower flow rates combined with high external oxygen atmospheres has the effect of essentially uncoupling the horizontally directed oxygen mass transport flux from the inlet flow, whilst maintaining a high vertical flux of oxygen from the PDMS membranes located along the top and bottom of the device.

3.6 Experimental data from proposed liver tissue device

The device geometry derived from the modelling was realised as described in the experimental section (Figs. 1 and 2, ESI2–4). Initial leak testing of the manufactured device with a red dye testing solution successfully demonstrated the sealing capabilities of the PDMS gas exchange membranes (figure S.4.1). Liver tissue sections were prepared as detailed

in the materials and methods and loaded into the device. The performance of the proposed device was compared against a static conventional tissue slice well plate approach by determining the amount of LDH retained in tissues following 72 h of incubation. The LDH levels found in the chips were approximately 30% and 16% of the levels of their respective PICMORG50 incubated controls, suggesting a lower level of viability (Fig. 10). However, these data must be considered preliminary as only two independent experiments were set up and there is a high level of variability in either set-up. Furthermore, there are well-known limitations regarding the measurement of LDH such as the release of enzyme inhibitors and interference from components of the media, thus a number of other such assays have been developed over the past years (Hattersley et al. 2008). Future studies will combine a number of these, alongside a time course of LDH release.

4 Conclusions

Mass transport of oxygen within tissue/organ-on-chip devices is an important parameter to achieve optimal maintenance and life-like conditions. We have investigated the suitability of several PCLS microfluidic devices for the adequate maintenance of oxygen mass transport using COMSOL simulations. This has led to the development of a novel, optimised, design to provide satisfactory in vivo oxygenation conditions within an organ-on-a-chip system. Simulations found that the proposed device was capable of maintaining 43% of the tissue volume within the physiological range of

Fig. 9 COMSOL simulation for the evaluation of the impact of the flow rate and oxygen gas composition upon the maintenance of the PCLS. **a** Illustration of the simulation geometry showing the positioning of the PCLS within the chip relative to the PDMS breathing windows. The PMMA frames of the chip and tissue unit are shown in grey and the nylon mesh is also coloured in grey. **b** Contour plot highlighting the interdependence of the inlet flow velocities and the applied oxygen atmospheres upon the effective oxygen tension experienced within a PCLS incubated in PDMS sandwich device. This simulation was conducted based on the assumption that the breathing window had an infinite width. Calculated values display the tissue volume percentages which are maintained in physiological range of the liver (0.042–0.091 mM) (colour figure online)
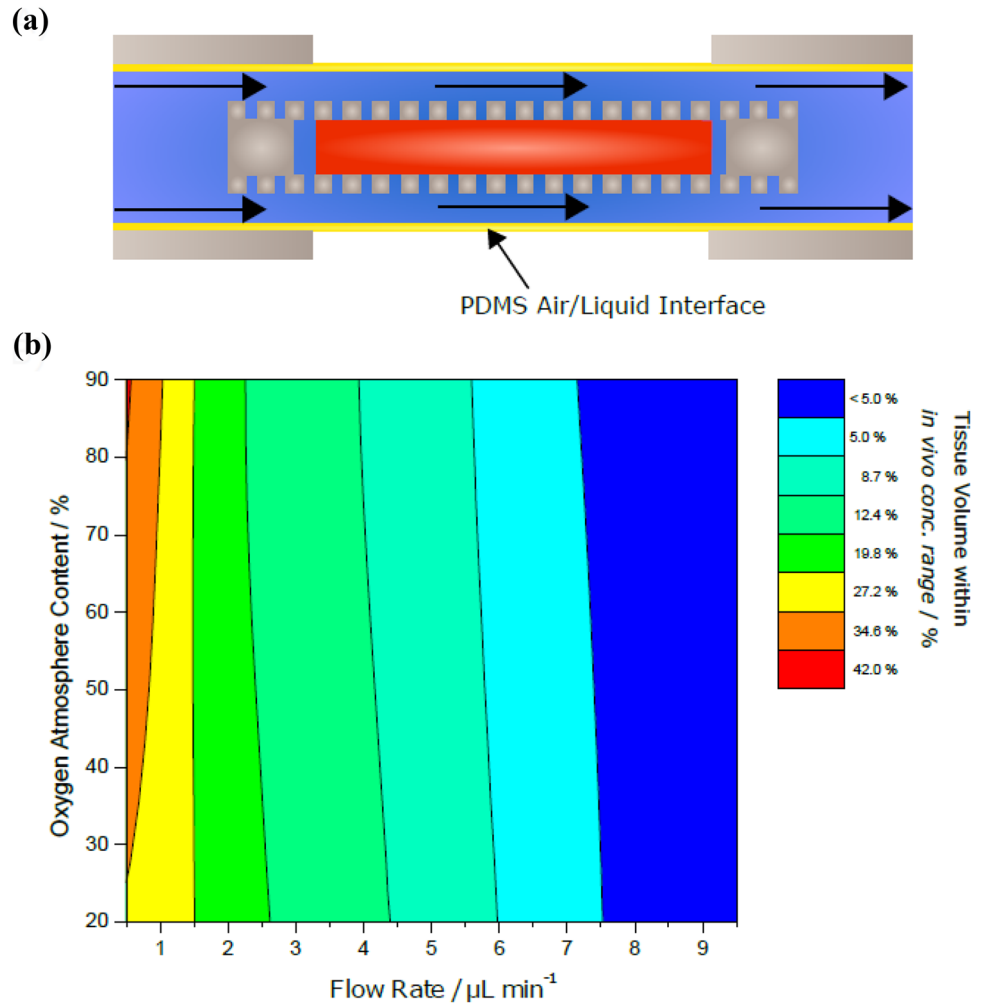
Fig. 10 Release of LDH into the effluents collected from PCLS incubated in PDMS sandwich device using a flow rate of 8 µL min^{-1} and PICMORG50 well plate controls run in parallel over a period of 72 h
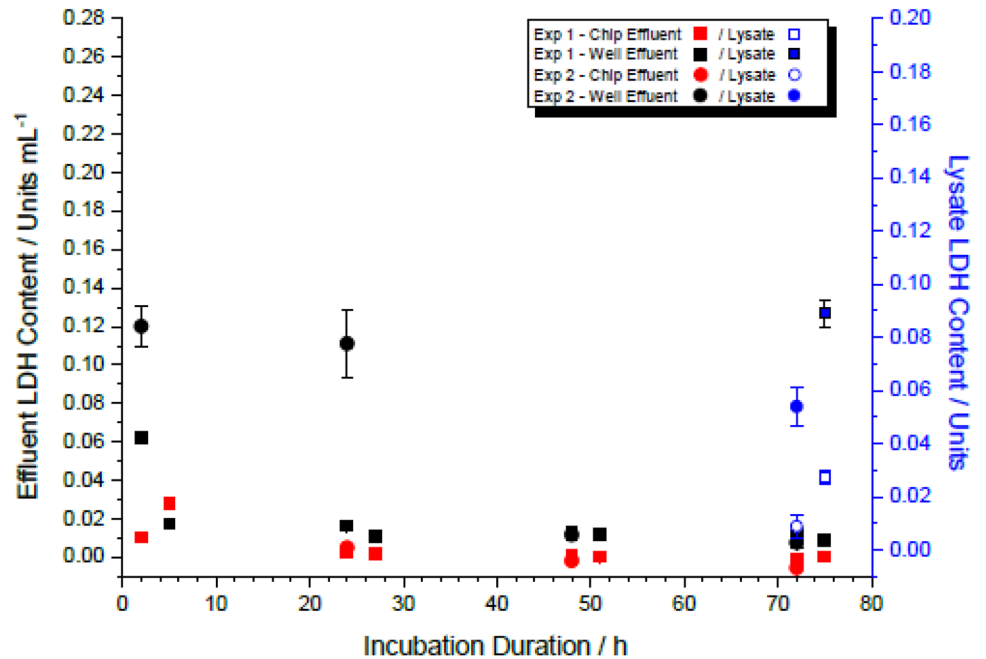
the liver against 18% for the best performing device reported in the literature. The optimised device was then fabricated and tested for LDH release to confirm its functioning. It would be possible to further increase the mass transfer capacity of the device by decreasing the channel height or increasing the gas atmosphere or adding oxygen carriers to the media. These simulation results form the basis for a greater understanding of not just the challenges involved in designing organ-on-a-chip devices, but also highlight issues that would arise from the incorporation of additional organs, as research progresses towards complete human-on-a-chip model systems.

References

Adams DJ (2012) The valley of death in anticancer drug development: a reassessment. Trends Pharmacol Sci 33(4):173–180

Astolfi M, Péant B, Lateef MA, Rousset N, Kendall-Dupont J, Carmona E et al (2016) Micro-dissected tumor tissues on chip: an ex vivo method for drug testing and personalized therapy. Lab Chip 16(2):312–325

Bedossa P, Paradis V (2003) Liver extracellular matrix in health and disease. J Pathol 200(4):504–515

Blake AJ, Pearce TM, Rao NS, Johnson SM, Williams JC (2007) Multilayer PDMS microfluidic chamber for controlling brain slice microenvironment. Lab Chip 7(7):842–849

Buchwald P (2011) A local glucose-and oxygen concentration-based insulin secretion model for pancreatic islets. Theor Biol Med Model 8(1):20

Buerk DG, Saidel GM (1978) Local kinetics of oxygen metabolism in brain and liver tissues. Microvasc Res 16(3):391–405

Camp JP, Capitano AT (2007) Induction of zone-like liver function gradients in HepG2 cells by varying culture medium height. Biotechnol Prog 23(6):1485–1491

Chang T, Monnat Jr RJ, Folch A (2012) A microfluidic device for exposing tumor biopsy tissue to multiple drugs. μTAS proceedings.

Chang TC, Mikheev AM, Huynh W, Monnat RJ, Rostomily RC, Folch A (2014) Parallel microfluidic chemosensitivity testing on individual slice cultures. Lab Chip 14(23):4540–4551

Cheng W, Klauke N, Sedgwick H, Smith GL, Cooper JM (2006) Metabolic monitoring of the electrically stimulated single heart cell within a microfluidic platform. Lab Chip 6(11):1424–1431

Cho M-H, Niles A, Huang R, Inglese J, Austin CP, Riss T, Xia M (2008) A bioluminescent cytotoxicity assay for assessment of membrane integrity. Toxicol In Vitro 22:1099–1106

De Graaf IA, Olinga P, De Jager MH, Merema MT, De Kanter R, Van De Kerkhof EG, Groothuis GM (2010) Preparation and incubation of precision-cut liver and intestinal slices for application in drug metabolism and toxicity studies. Nat Protoc 5(9):1540

Esch MB, Smith AS, Prot JM, Oleaga C, Hickman JJ, Shuler ML (2014) How multi-organ microdevices can help foster drug development. Adv Drug Deliv Rev 69:158–169

Ges IA, Baudenbacher F (2010a) Enzyme-coated microelectrodes to monitor lactate production in a nanoliter microfluidic cell culture device. Biosens Bioelectron 26(2):828–833

Ges IA, Baudenbacher F (2010b) Enzyme electrodes to monitor glucose consumption of single cardiac myocytes in sub-nanoliter volumes. Biosens Bioelectron 25(5):1019–1024

Graaf IAD, Groothuis GM, Olinga P (2007) Precision-cut tissue slices as a tool to predict metabolism of novel drugs. Expert Opin Drug Metab Toxicol 3(6):879–898

Guo R, Xu X, Lu Y, Xie X (2017) Physiological oxygen tension reduces hepatocyte dedifferentiation in in vitro culture. Sci Rep 7(1):5923

Gupta RC (2018) Veterinary toxicology: basic and clinical principles (3rd Edition). ISBN-13: 978–0128114100

Hattersley SM, Dyer CE, Greenman J, Haswell SJ (2008) Development of a microfluidic device for the maintenance and interrogation of viable tissue biopsies. Lab Chip 8(11):1842–1846

Hiatt LA, McKenzie JR, Deravi LF, Harry RS, Wright DW, Cliffel DE (2012) A printed superoxide dismutase coated electrode for the study of macrophage oxidative burst. Biosens Bioelectron 33(1):128–133

Iorga A, Dara L, Kaplowitz N (2017) Drug-induced liver injury: cascade of events leading to cell death, apoptosis or necrosis. Int J Mol Sci 18(5):1018

Ivanovic Z (2009) Hypoxia or in situ normoxia: the stem cell paradigm. J Cell Physiol 219(2):271–275

Jungermann K, Keitzmann T (1996) Zonation of parenchymal and nonparenchymal metabolism in liver. Annu Rev Nutr 16(1):179–203

Jungermann K, Kietzmann T (2000) Oxygen: modulator of metabolic zonation and disease of the liver. Hepatology 31(2):255–260

Khong YM, Zhang J, Zhou S, Cheung C, Doberstein K, Samper V, Yu H (2007) Novel intra-tissue perfusion system for culturing thick liver tissue. Tissue Eng 13(9):2345–2356

Kullak-Ublick GA, Andrade RJ, Merz M, End P, Benesic A, Gerbes AL, Aithal GP (2017) Drug-induced liver injury: recent advances in diagnosis and risk assessment. Gut 66(6):1154–1164

Mattei G, Giusti S, Ahluwalia A (2014) Design criteria for generating physiologically relevant in vitro models in bioreactors. Processes 2(3):548–569

Misun PM, Rothe J, Hierlemann A, Frey O (2015) Real-time multi-analyte online monitoring of 3d cell cultures by integrated enzyme-based biosensors in hanging drop networks. Transducers 18th International Conference on Solid-State Sensors, Actuators and Microsystems: 1625–1628. IEEE

Misun PM, Rothe J, Schmid YR, Hierlemann A, Frey O (2016) Multi-analyte biosensor interface for real-time monitoring of 3D microtissue spheroids in hanging-drop networks. Microsyst Nanoeng 2:16022

Ortega-Prieto AM, Skelton JK, Wai SN, Large E, Lussignol M, Vizcay-Barrena G et al (2018) 3D microfluidic liver cultures as a physiological preclinical tool for hepatitis B virus infection. Nat Commun 9(1):682

Patel SJ, Milwid JM, King KR, Bohr S, Iracheta-Vellve A, Li M et al (2012) Gap junction inhibition prevents drug-induced liver toxicity and fulminant hepatic failure. Nat Biotechnol 30(2):179–183

Rambani K, Vukasinovic J, Glezer A, Potter SM (2009) Culturing thick brain slices: an interstitial 3D microperfusion system for enhanced viability. J Neurosci Methods 180(2):243–254

Rodrigues NP, Sakai Y, Fuji T (2008) Cell-based microfluidic biochip for the electrochemical real-time monitoring of glucose and oxygen. Sensors Actuators B Chem 132(2):608–613

Sivashankar S, Puttaswamy SV, Lin HL, Yang SM, Chen HP, Yeh CT, Liu CH (2012) 3D microstructure integrated bioreactor system for transgenic mice thick liver tissue culture. 7th International Conference on Nano/Micro Engineered and Molecular Systems (NEMS): 158–161. IEEE

Usta OB, McCarty WJ, Bale S, Hegde M, Jindal R, Bhushan A et al (2015) Microengineered cell and tissue systems for drug screening and toxicology applications: Evolution of in-vitro liver technologies. Technology 3(01):1–26

van Midwoud PM, Merema MT, Verpoorte E, Groothuis GM (2010) A microfluidic approach for in vitro assessment of interorgan interactions in drug metabolism using intestinal and liver slices. Lab Chip 10(20):2778–2786

van Midwoud PM, Merema MT, Verweij N, Groothuis GM, Verpoorte E (2011) Hydrogel embedding of precision-cut liver slices in a microfluidic device improves drug metabolic activity. Biotechnol Bioeng 108(6):1404–1412

Visk D (2015) Will advances in preclinical in vitro models lower the costs of drug development? Appl In Vitro Toxicol 1(1):79–82

Wells RG (2013) Tissue mechanics and fibrosis. BBA 1832(7):884–890

Weltin A, Slotwinski K, Kieninger J, Moser I, Jobst G, Wego M et al (2014) Cell culture monitoring for drug screening and cancer research: a transparent, microfluidic, multi-sensor microsystem. Lab Chip 14(1):138–146

Wu C W, Sivashankar S, Puttaswamy SV, Lin HL, Chang KW, Yeh CT, Liu CH (2012) In-vitro transgenic mice liver tissue culture via hydrodynamic flow perfusion bioreactor. 7th International Conference on Nano/Micro Engineered and Molecular Systems (NEMS): 133–136. IEEE